Giant Nonlinear Optical Activity of Achiral Origin in Planar Metasurfaces with Quadratic and Cubic Nonlinearities

Shumei Chen, Franziska Zeuner, Martin Weismann, Bernhard Reineke, Guixin Li, Ventsislav Kolev Valev, Kok Wai Cheah, Nicolae Coriolan Panoiu, Thomas Zentgraf,* and Shuang Zhang**

In plasmonic nanomaterials, light can excite coherent oscillations of the surface electrons, which lead to strongly enlarged electromagnetic near-fields. Such enlargements are useful to enhance the light-mater interaction with chiral molecules,[1–3] leading to vast improvements in sensitivity to the chiral purity of pharmaceuticals, agrochemicals, biomolecules, etc. Chiral plasmonic nanomaterials in particular have been investigated for their selective interaction with circularly polarized light, which can enable, for instance, highly localized control of circularly polarized light emission. As we will see though, chirality is not a necessary condition for exercising such a control, or for having a different interaction with the two directions of circularly polarized light in general. Such difference in interaction is referred to as "optical activity".

Optical activity has been successfully employed for probing the symmetry of chemical surfaces, biomaterials, and crystals.[4,5] As the two manifestations of optical activity, optical rotatory dispersion and circular dichroism (CD) arise from phase and absorption differences between left- and right-circularly polarized light (LCP and RCP, respectively), when they pass through the chiral media. Usually, these two effects are very weak in natural materials. In comparison to the weak chiral phenomena in linear optical regime, optical activity for higher-harmonic generation exhibits much higher contrast for the two circular polarizations.[6–8] Therefore, second harmonic generation circular dichroism (SHG-CD) has become a powerful technique to probe the symmetry of organic and inorganic materials due to its high sensitivity to the asymmetry of molecules and physical interfaces.[9–11] In recent years, there has been a growing interest in the investigation of the nonlinear properties of plasmonic nanostructures and optical metamaterials, due to the associated strong enhancements of electromagnetic fields and to the capability to engineer the structural symmetry of their unit cell.[12–15] In particular, nonlinear optical CD of metamaterial and plasmonic nanostructures have been demonstrated.[16–23] However, the observed nonlinear optical CD in most experiments arises either from the chirality in 3D nanostructures, or from the extrinsic contribution in the case of 2D structures when the fundamental beam is incident at oblique angles. It should be pointed out that even seemingly 2D chiral materials, such as monolayers of chiral thin-film nanostructures are intrinsically 3D chiral as recently demonstrated in the linear[24] and in the nonlinear optical regimes.[23] In such nanostructures, chirality arises from the presence of a substrate on one side of the thin-films and not on the other.

Here, we demonstrate giant circular dichroism for both second and third harmonic generation on ultrathin plasmonic metasurfaces with broken in-plane mirror symmetry. Despite the symmetry breaking along surface normal direction due to the presence of substrate, this dichroism is primarily of achiral origin. The result is verified by the measurements of harmonic generation for circularly polarized fundamental beam at normal incidence from both the front (air) and back (substrate) sides. This strong nonlinear CD of achiral origin is explained by the effective nonlinear susceptibility coefficients associated with the specific C3 and C4 rotational symmetries of Triscelion- and Gammadion-type plasmonic nanostructures, which only involve the in-plane tensor elements. As shown schematically in **Figure 1**, the magnitude of the measured nonlinear CD for SHG and for third harmonic generation (THG) reaches near the maximum theoretical limit. Additionally, we show that upon illumination with left- or right-handed circularly polarized light, the C3 and C4 rotational symmetric nanostructures can generate cross-polarized SHG and THG waves, respectively.

To maintain the rotational symmetry of the overall experimental configuration, we limit ourselves to the configuration in which the fundamental wave is incident normally onto the surface. Therefore, the relevant effective nonlinear susceptibility tensor elements are those with sub-indices consisting only of x and y, assuming a Cartesian coordinate system, where the sample is in the x–y plane. Due to the rotational symmetry

Dr. S. Chen, Dr. G. Li, Prof. S. Zhang
School of Physics and Astronomy
University of Birmingham
Birmingham B15 2TT, UK
E-mail: s.zhang@bham.ac.uk
Dr. S. Chen, Prof. K. W. Cheah
Department of Physics
Hong Kong Baptist University
Kowloon Tong, Hong Kong
F. Zeuner, B. Reineke, Prof. T. Zentgraf
Department of Physics
University of Paderborn
Warburger Straße 100, Paderborn D-33098, Germany
E-mail: thomas.zentgraf@upb.de
M. Weismann, Dr. N. C. Panoiu
Department of Electronic and Electrical Engineering
University College London
Torrington Place, London WC1 E7JE, UK
E-mail: n.panoiu@ucl.ac.uk
Dr. V. K. Valev
Department of Physics
University of Bath
Claverton Down, Bath BA2 7AY, UK

DOI: 10.1002/adma.201505640

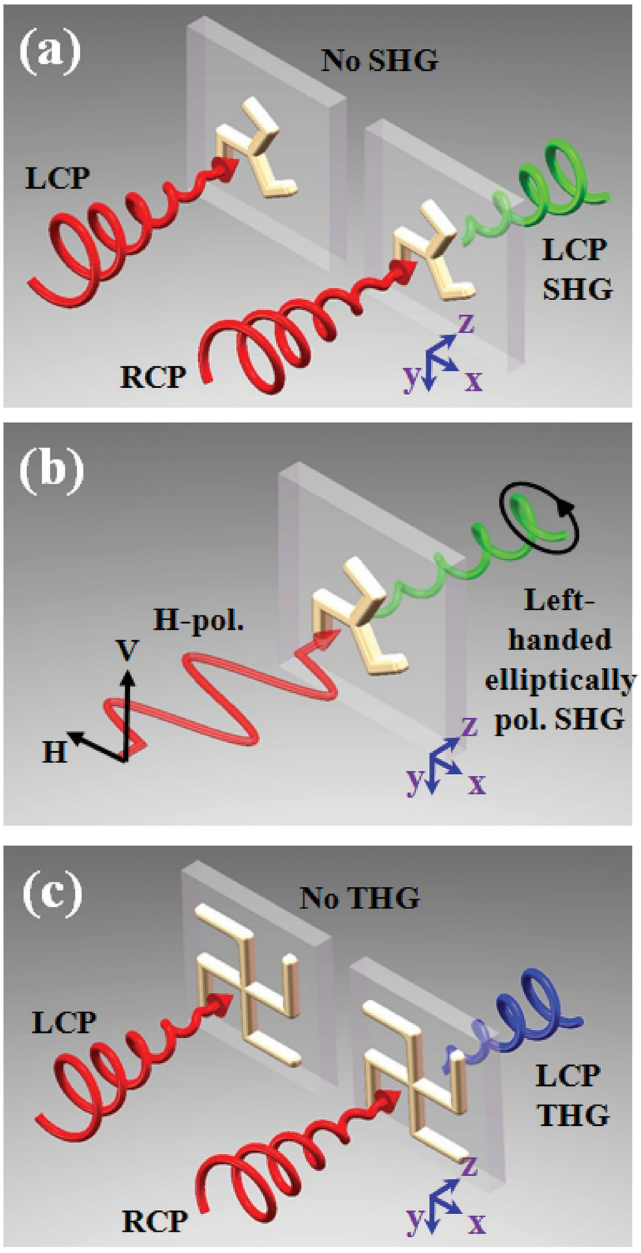

Figure 1. Schematic of nonlinear optical dichroism from Trisceli- and Gammadion-type plasmonic nanostructures with three- (C3) and four-fold (C4) rotational symmetries. (a) and (c) illustrate the nonlinear circular dichroism for illumination with LCP and RCP polarizations on such structures which will lead to SHG and THG with opposite polarizations but only for the RCP illumination. Trisceli-type nanostructures with near unity SHG-CD shown in (b) would generate left-handed elliptically polarized SHG light when illuminated by linear polarized light.

of both the individual structure and the lattice, the effective nonlinear susceptibility tensor can be reduced to just a few independent elements.

We start with the second-order nonlinear susceptibility tensor for the metasurfaces consisting of nanostructures with C3 rotational symmetry. It has been shown that the C3 rotational symmetry reduces the tensor elements to two independent values: $\chi_{yyy}=-\chi_{yxx}=-\chi_{xxy}=-\chi_{xyx}=\chi_1$, $\chi_{xxx}=-\chi_{xyy}=-\chi_{yyx}=-\chi_{yxy}=\chi_2$.[25]

In contrast, for previously investigated crystal surfaces possessing C_{3v} symmetry, such as Si (111) and GaAs (111), both the rotational symmetry and mirror symmetry are present and only a single tensor element is nonzero depending on whether x or y is aligned with one of the symmetry planes. Thus, for the C3 structure investigated here, the effective nonlinear polarization can be expressed as:

$$P_x^{2\omega}=\varepsilon_0\chi_2(E_x^2-E_y^2)-2\varepsilon_0\chi_1E_xE_y \quad (1)$$

$$P_y^{2\omega}=-2\varepsilon_0\chi_2E_xE_y-\varepsilon_0\chi_1(E_x^2-E_y^2) \quad (2)$$

For a circularly polarized incident beam, the electric field vector is given by $\vec{E}=E_0(\hat{e}_x\pm i\hat{e}_y)/\sqrt{2}$, where the "+" and "–" sign correspond to LCP and RCP, respectively. Here we use the definition of LCP and RCP as defined from the point of view of the receiver. The effective nonlinear polarization can be expressed as

$$\vec{P}^{2\omega}=(\chi_2\mp i\chi_1)(\hat{e}_x\mp i\hat{e}_y)\varepsilon_0E_0^2 \quad (3)$$

This equation agrees with the selection rule studied previously, circularly polarized light cannot produce the SHG with the same polarization as the fundamental light at normal incidence onto a structure with C3 symmetry.[26–30] In addition, Equation (3) shows that the intensities of the SHG are generally different for the two circular polarization states. However, to obtain a difference in the SHG intensity for the two circular polarization states it is necessary that χ_1 and χ_2 are different in phase. Note that if χ_1 and χ_2 have the same phase, a coordinate rotation can be employed to reduce the in-plane nonlinear coefficients to a single one $\chi=\sqrt{\chi_1^2+\chi_2^2}$, i e., the system becomes the same as for a C_{3v} symmetry. The highest contrast between the two circular polarization states can be achieved in the case that χ_1 and χ_2 are equal in amplitude and $\pi/2$ out of phase. This would lead to a unity SHG-CD, which arises from the cancellation of the nonlinear polarization between the contributions from χ_1 and χ_2 for one circular polarization state, but a constructive interference between their contributions for the other circular polarization. The above analysis shows that, for a nanostructured thin film with C_3 rotational symmetry, nonlinear susceptibility tensor components with z indices are not necessary for introducing nonlinear CD for second-harmonic generations. This is in stark contrast to commonly studied SHG-CD effect in chiral thin films.[31]

For an incident wave with linear polarization along the horizontal direction $(E_x,\ E_y)=(E_0,\ 0)$, we have $P_x^{2\omega}=\varepsilon_0\chi_2E_0$ and $P_y^{2\omega}=-\varepsilon_0\chi_1E_0$. If an analyzer is placed in transmission with orientation angle θ, the measured SHG intensity is given by:

$$I_\theta^{2\omega}\propto\left|P_\theta^{2\omega}\right|^2\propto\left|\chi_2\cos\theta-\chi_1\sin\theta\right|^2 \quad (4)$$

By normalizing χ_1 to unity and setting $\chi_2=a\exp(i\varphi)$, the above equation can be rewritten in a simple sinusoidal form as:

$$I_\theta^{2\omega}\propto 1-\cos\beta\sin(2\theta+\delta) \quad (5)$$

where $\beta=\sin^{-1}\left(2a\sin\varphi/(1+a^2)\right)$ and $\delta=\tan^{-1}\left((a^2-1)/2a\cos\varphi\right)$.

Interestingly, based on Equation (3) and the definition of β, SHG-CD can be derived as:

$$\mathrm{CD} = \frac{I_{\mathrm{LCP}}^{2\omega} - I_{\mathrm{RCP}}^{2\omega}}{I_{\mathrm{LCP}}^{2\omega} + I_{\mathrm{RCP}}^{2\omega}} = \sin\beta \tag{6}$$

Thus, Equation (5) and (6) show that the circular dichroism for SHG can be independently obtained by two measurements – the ellipticity of the SHG for a linearly polarized fundamental beam, or a direct measurement of the relative difference between the SHG signals of the two opposite circularly polarized incident fundamental beams. It shall be shown later that both measurements are carried out and show highly consistent results. The SHG measurement is also carried out on the C4 sample (see the Supporting Information). For the same experimental geometry, and whereas both sample arrays break the in-plane mirror symmetry, the SHG signal in the C4 case is several orders of magnitude smaller than that in the C3 case due to the violation of the selection rule pertaining to the harmonic generation of circularly polarized light.[26–30]

For THG processes, applying a C4 rotational symmetry reduces the third-order nonlinear tensors to four independent elements. Hence, the third-order nonlinear polarization can be expressed as:

$$\begin{aligned} P_x^{3\omega} &= \varepsilon_0[\chi_1 E_x^3 + \chi_2 E_x E_y^2 + \chi_3 E_x^2 E_y + \chi_4 E_y^3] \\ P_y^{3\omega} &= \varepsilon_0[\chi_1 E_y^3 + \chi_2 E_y E_x^2 - \chi_3 E_y^2 E_x - \chi_4 E_x^3] \end{aligned} \tag{7}$$

where $\chi_1 = \chi_{xxxx}$, $\chi_2 = \chi_{xxyy} + \chi_{xyxy} + \chi_{xyyx}$, $\chi_3 = \chi_{xxxy} + \chi_{xxyx} + \chi_{xyxx}$, and $\chi_4 = \chi_{xyyy}$.[25] For left- and right-circularly polarized fundamental waves, the nonlinear polarization at the TH wavelength is then given by:

$$\vec{P}^{3\omega} \propto \frac{1}{2}[(\chi_1 - \chi_2) \mp i(\chi_3 - \chi_4)](\hat{e}_x \mp i\hat{e}_y) \tag{8}$$

Again, this equation agrees with the selection rule for THG.[26–30] Furthermore, Equation (8) shows that there would exist THG-CD for a C4 plasmonic nanostructure if (χ_3–χ_4) is out of phase with (χ_1–χ_2).

The nonlinear optical response of the metasurfaces at the TH wavelength has been numerically calculated using a recently developed numerical method,[32] which extends the generalized-source method (GSM)[33] to nonlinear optical interactions. This nonlinear GSM provides a general computational framework that can be easily adapted to a broad class of nonlinear optical interactions, as the system nonlinearity is incorporated in the algorithm via nonlinear polarizations acting as sources for the nonlinear optical field. More specifically, the nonlinear optical response of the system is obtained in three steps: one determines first the optical field at the fundamental wavelength using the linear GSM, then one calculates the nonlinear polarizations describing the corresponding nonlinear optical processes, and finally one adds these polarizations to the linear polarization and use again the linear GSM to compute the nonlinear optical fields and other optical coefficients. This computational approach ensures that the influence of the electromagnetic environment on the radiative characteristics of the nonlinear sources is rigorously taken into account.

Specifically, the nonlinear optical response of the system at the TH wavelength is described by a spatially varying bulk polarization $\vec{P}^{3\omega}(\vec{r}) = \varepsilon_0 \chi^{(3)}(\vec{E}(\vec{r}) \cdot \vec{E}(\vec{r}))\vec{E}(\vec{r})$, which depends on the complex field $\vec{E}(\vec{r})$ and the nonlinear susceptibility $\chi^{(3)}$ of the respective material at the location $\vec{r}$. In particular, it is assumed that the optical nonlinearity of the medium is homogeneous and isotropic, so that the nonlinear third-order susceptibility tensor is described by a single quantity. The numerical values of this susceptibility in the cases of Gold[34], PFO[35], and ITO[36] are $\chi_{\mathrm{gold}}^{(3)} = 5.58 \times 10^{-20}\,\mathrm{m^2V}$, $\chi_{\mathrm{PFO}}^{(3)} = \chi_{\mathrm{gold}}^{(3)}$ and $\chi_{\mathrm{ITO}}^{(3)} = 1.0 \times 10^{-20}\,\mathrm{m^2V}$, respectively. The linear material dispersion parameters can be found in refs.[37,38].

In the case of SHG, the convergence of GSM is very slow due to the fact that the nonlinear effects come from the interfaces between gold and the surrounding dielectric media (air and glass). Instead, we follow the method proposed by O'Brien et al., in which the SHG is calculated by an overlapping integral between the nonlinear polarization at the metal-dielectric interfaces and the near field distribution of the electric field when the metasurface is illuminated by a plane wave at the second harmonic frequency.[39,40]

From symmetry selection rules of harmonic generation, it is known that nanostructures with C3 and C4 symmetries can generate circularly polarized SHG and THG signals with opposite polarizations as compared to the fundamental wave. The Trisceli- and Gammadion-type plasmonic nanostructures are fabricated on ITO coated BK7 glass substrates by using electron-beam lithography and a lift-off process (see the Experimental Section). As shown in **Figure 2**a,b, these two types of gold nanostructures with thickness of 30 nm are arranged in triangular and square lattices with periods of 400 and 500 nm, respectively. The Gammadion nanostructures are subsequently covered by a thin layer of an organic conjugated polymer (PFO) with high third-order optical nonlinearity to enhance the efficiency of THG. Figure 2c,d shows the measured transmission spectra of the plasmonic nanostructures for horizontally polarized incident and transmitted light (HH) by using Fourier transform infrared spectrometer. The dips in the transmission spectra correspond to the excitation of localized surface plasmon polariton modes of the Trisceli- and Gammadion-type plasmonic nanostructures at wavelength of 1165 and 1230 nm, respectively, which are also confirmed by the numerical simulations.

In most conventional SHG-CD measurements, oblique incidence of light is usually employed to project a strong electric field component of light along the z direction of the sample. This geometry allows access to nonlinear susceptibility tensor components with one or several z indices, which can be quite large in some materials.[4,5] In particular, the so-called chiral tensor components contain such z indices. Since we seek to minimize the chiral contribution to SHG-CD and to emphasize an achiral SHG-CD instead, here, we use a femtosecond laser beam under normal incidence to the sample surface to interact with the nanostructures. Moreover, we used a low numerical aperture objective (NA = 0.1 to minimize the projection of a polarization component along the propagation direction. The signals of harmonic generation are then collected

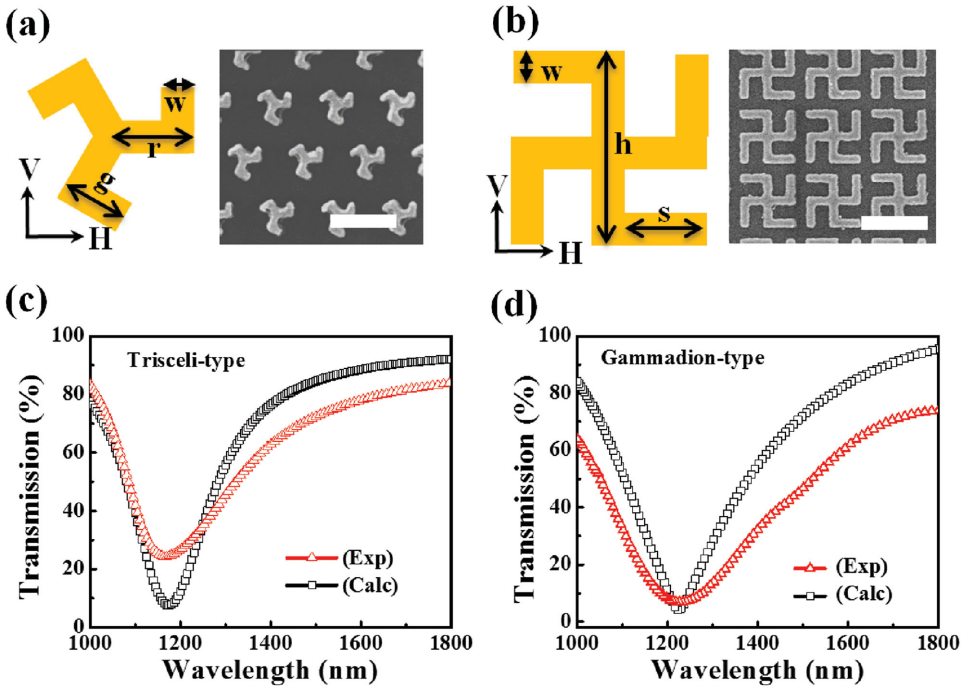

Figure 2. Geometry parameters and transmission properties of the plasmonic nanostructures. a,b) Schematic view of single Trisceli- and Gammadion-type plasmonic nanostructures and scanning electron microscopy images of the fabricated periodic pattern (scale bar: 500 nm). The 30 nm thick gold structures are arranged in triangular and square lattices with periods of 400 and 500 nm, respectively. The geometry parameters of the gold nanostructures are $w = 60$ nm, $r = 110$ nm, $g = 100$ nm, $h = 410$ nm, and $s = 175$ nm. c and d) Measured ("Exp") linear transmission spectra of the Trisceli- and PFO-coated Gammadion-type nanostructures for linearly (horizontally) polarized light, exhibiting localized plasmon resonance at wavelength of 1165 and 1230 nm, respectively, which agree well with the calculated ("Calc") transmission spectra.

in the transmission direction. To characterize the frequency dependent nonlinear optical activity, the wavelength of illuminating laser is tuned between $\lambda_o = 1100$ and 1400 nm and the circularly polarized SHG and THG signals are recorded with a spectrometer (**Figure 3**a,d). We found that SHG and THG signals from the plasmonic nanostructures have opposite polarization states as compared to that of the illuminating laser. However, we also measured extremely low SHG and THG with the same polarization state as that of the illuminating laser although they are theoretically forbidden in the dipole approximation but can be observed due to the imperfections of nanofabrication.[21,22] For the SHG measurements, both the L–R and R–L spectra increase with wavelength up to 1160 nm. However, the L–R intensity drops abruptly with further increasing wavelength above 1160 nm, while the R–L intensity keeps further increasing and peaks around 1220 nm. As a result, there exists a large difference between the SHG intensities for the two circularly polarized incident beams for wavelength above 1160 nm. Particularly, at around 1280 nm wavelength, the SHG for the illumination with LCP light (L–R) drops almost to zero while that for the illumination with RCP light (R–L) is very strong, leading to near unity value of 0.98 for SHG-CD at this wavelength.

Our measurements nicely confirm numerical simulations of the SHG and THG signals from such structures, which also predict large differences between the two polarized signals (Figure 3b,e). The measured nonlinear spectra of the SHG intensity show similar features as those of calculated SHG spectra. The slight discrepancy between the experiment and the simulation might be due to both the deviation of the fabricated sample from the ideal design, and the limited precision of the simulation of the nonlinear signals due to their extreme sensitivity to the local field distribution.

In an ideal achiral configuration of free standing C3 nanostructures without the presence of substrate, it is expected that when the sample is flipped between the front and reverse-side, SHG spectra are swapped between the two circular polarizations, i.e., $I^{f}_{R\to L}(2\omega) = I^{b}_{L\to R}(2\omega)$ and $I^{f}_{L\to R}(2\omega) = I^{b}_{R\to L}(2\omega)$, where "f" and "b" correspond to front- and back-illumination of the fundamental wave, respectively. This is because flipping the sample leads to a change of sign for either χ_1 or χ_2 (depending on flipping the sample by rotating along x or y axis), but not both, and consequently results in reversal of the CD effect based on Equation (3). However, in the realistic case, the nanostructures are supported by a substrate which breaks the symmetry along the z direction. To investigate into the role of the symmetry breaking in the z direction due to the presence of substrate on SHG-CD, we perform an additional SHG measurement on C3 sample, now flipped such that the fundamental beam is incident from the substrate side, with the spectra shown in Figure 3c. As can be seen from the figure, flipping the sample leads to exchange of the SHG spectra between the two circularly polarized fundamental waves. This observation serves as direct evidence that the observed SHG-CD is mainly due to the in-plane symmetry breaking alone, which is of achiral nature.

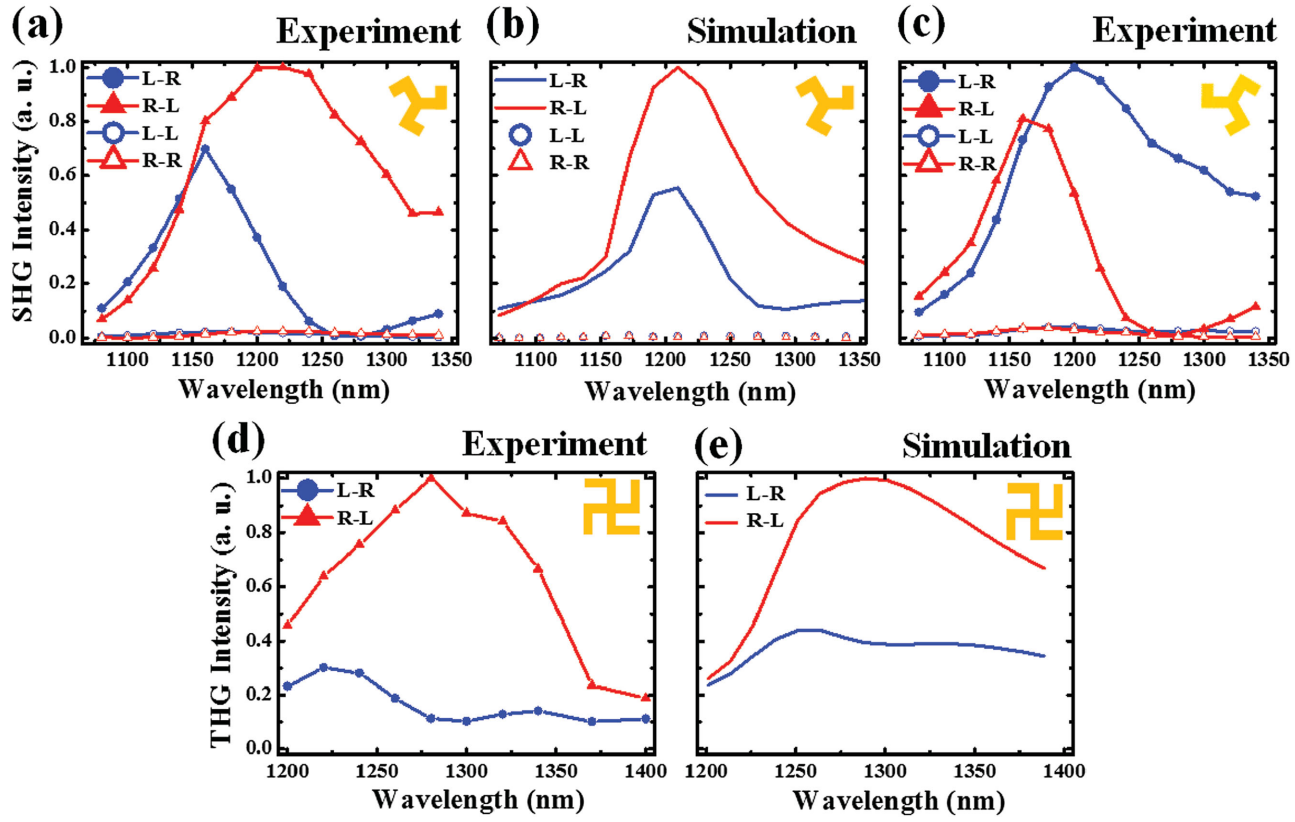

Figure 3. Polarization-dependent SHG and THG spectra of the Trisceli- and Gammadion-type plasmonic nanostructures. Measured SHG and THG spectra with same (LCP–LCP and RCP–RCP) and opposite circular polarizations (LCP–RCP and RCP–LCP) as that of the illuminating light. Note, in the figure we used the abbreviation of L for LCP and R for RCP, respectively. a,b) Measured (a) and numerically simulated (b) SHG spectra for fundamental wave normally incident from Trisceli-type nanostructure direction to substrate direction (front illumination). It is found that SHG for R–L and L–R measurements exhibit significant difference when fundamental wavelength is greater than 1160 nm, whereas L–L is close to R–R. c) Measured SHG spectra for light incident from the substrate side (back illumination), which are very close to the results of front illumination but swapped between R–L and L–R. d,e) Measured (d) and simulated (e) THG spectra under front illumination show pronounced difference between R–L and L–R for fundamental wavelength with a bandwidth of around 150 nm.

For the C4 sample, the THG spectra also show pronounced difference between the two circular polarization states over a broad frequency range between 1200 and 1400 nm (Figure 3d). While the THG spectrum for the R–L configuration exhibits a peak around 1280 nm wavelength, the L–R spectrum is almost featureless over the entire frequency range. The THG intensity of the R–L configuration is approximately one order of magnitude greater than that of the L–R configuration at 1280 nm. Again, the simulation of the THG signals exhibits similar features to those of the experimental results. However, the relative differences between the THG of the two circular polarizations are not as large as the measured values.

Based on the measured spectral results for both SHG and THG, as shown in **Figure 4**a,c, we calculated the nonlinear CDs by $(I_{LCP} - I_{RCP})/(I_{LCP} + I_{RCP})$. The SHG-CD varies from negative to positive values, crossing zero around 1150 nm and reaching near-unity value of 0.98 at 1280 nm. On the other hand, the THG-CD reaches its maximum value of 0.79 at 1280 nm. We note that this is the first observation of THG-CD on planar chiral plasmonic structures. Furthermore, the maximum value of the measured nonlinear SHG-CD is much higher than that of the linear CD effect observed previously from the Gammadion-type plasmonic nanostructures.[24] We also found very similar trends of the nonlinear CDs from the simulated SHG and THG signals (Figure 4b,d), where the simulated maximum values of the SHD-CD and the THG-CD are 0.637 at 1271 nm and 0.435 at 1301 nm, respectively. These values are somewhat lower than their respective measured values.

Above we showed that the nonlinear CD has to be related to the nonlinear susceptibility tensor elements. In order to retrieve the effective susceptibilities of the SHG from the Trisceli-type nanostructures, the SHG intensity as function of the rotational angle of the analyzer is measured for four different wavelengths: 1160, 1180, 1220, and 1280 nm, for a fixed linear polarization of the illuminating light along the vertical direction. As illustrated in **Figure 5**, the SHG intensities show a sinusoidal dependence on the analyzer angle. At the shortest wavelength of 1160 nm, the minimum value is close to zero, indicating that the SHG signal is linearly polarized at this wavelength. With the increase of wavelength, the minimum value rises, indicating the increase of the SHG ellipticity. This is consistent with the observation of vanishing SHG-CD at 1150 nm and its increase up to 1280 nm, as shown in Figure 4. By using Equation (1) and (2), we can fit the curves and retrieve the

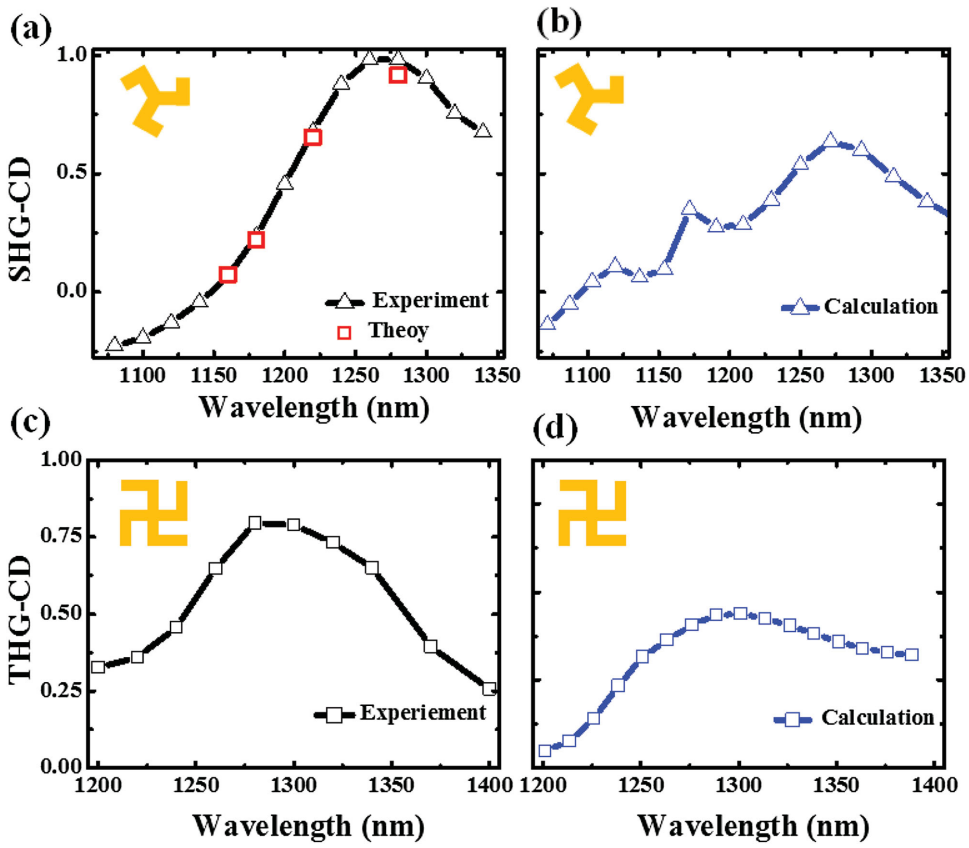

Figure 4. SHG-CD and THG-CD from the Trisceli- and Gammadion-type plasmonic nanostructures. a,c) Measured (Exp) wavelength-dependent SHG-CD and THG-CD. The values for the squares in (a) are obtained from the calculation (Calc) of SHG-CD based on the experimentally determined values of the effective nonlinear susceptibilities. Both SHG-CD and THG-CD have a broadband response for fundamental wavelength between 1200 and 1350 nm. The SHG-CD experiences a sign change at wavelength of ≈1150 nm, which is close to the theoretical prediction of 1100 nm. b,d) Corresponding numerically simulated (Simulation) nonlinear CD spectra for the structures. Both of the calculated SHG and THG spectra show similar trend as the measured ones. While the peak of SHG-CD is close to the measured value, the calculated THG has a much higher deviation from our experimental data, which can be attributed to the imperfections of nanofabrication.

values of χ_2 with χ_1 being normalized to 1. This normalization of χ_1 is well justified since we are only interested in the structural effect but not the absolute nonlinear signal strength, and consequently only the ratio between χ_2 and χ_1 is of relevance (absolute values are given in the Supporting Information). From this retrieval we obtain for χ_2: −4.5 + 0.8i, −2 + 0.6i, −0.9 + 0.8i, and −0.13 + 0.68i for the fundamental waves at wavelength of 1160, 1180, 1220, and 1280 nm, respectively. Based on Equation (3) and the fitted values of χ_1 and χ_2, we numerically calculate the SHG-CD (red squares in Figure 4a), which agrees very well with the directly measured SHG-CD. Thus, with two independent measurements, we confirm the presence of near-unity SHG-CD at wavelength of 1280 nm for planar chiral nanostructures.

In summary, we demonstrate near-unity nonlinear circular dichroism for both second and third harmonic generations with suitably designed ultrathin Trisceli- and Gammadion-type plasmonic nanostructures with three- and four-fold rotational symmetry. These two kinds of nanostructures allow a symmetry controlled generation of circularly polarized SHG and THG, respectively. Both giant SHG-CD and THG-CD are experimentally observed for the planar plasmonic nanostructures with negligible linear optical activity. Importantly, the observed SHG-CD is identified to have an achiral origin. The simple fabrication of 2D plasmonic structures and wider applicability of SHG and THG techniques also enable more freedoms in designing chip-type nonlinear optoelectronic devices.

Experimental Section

Sample Fabrication: The plasmonic nanostructures were fabricated using e-beam lithography method. Firstly, the 150 nm thick PMMA layer was spin coated onto the ITO-coated (≈15 nm) BK-7 glass substrate. The 2D Trisceli and Gammadion patterns were exposed by e-beam lithography process. Then the 30 nm thick gold film was deposited on the patterned PMMA layer by using thermal evaporation. After removing the residue resist using acetone solvent, the 2D gold nanostructures with C3 and C4 rotational symmetries were formed. The total area size of the plasmonic device was ≈0.01 and 0.25 mm^2 for the Trisceli- and Gammadion-type devices, respectively. The Gammadion-type nanostructures was spin coated by a 100 nm thick organic thin film from the PFO solution dissolved in toluene with a concentration of 12 mg mL^{-1}.

Nonlinear Optical Experiments: Spectrally tunable femtosecond laser pulses (1.1–1.4 μm) from an optical parametric oscillator system

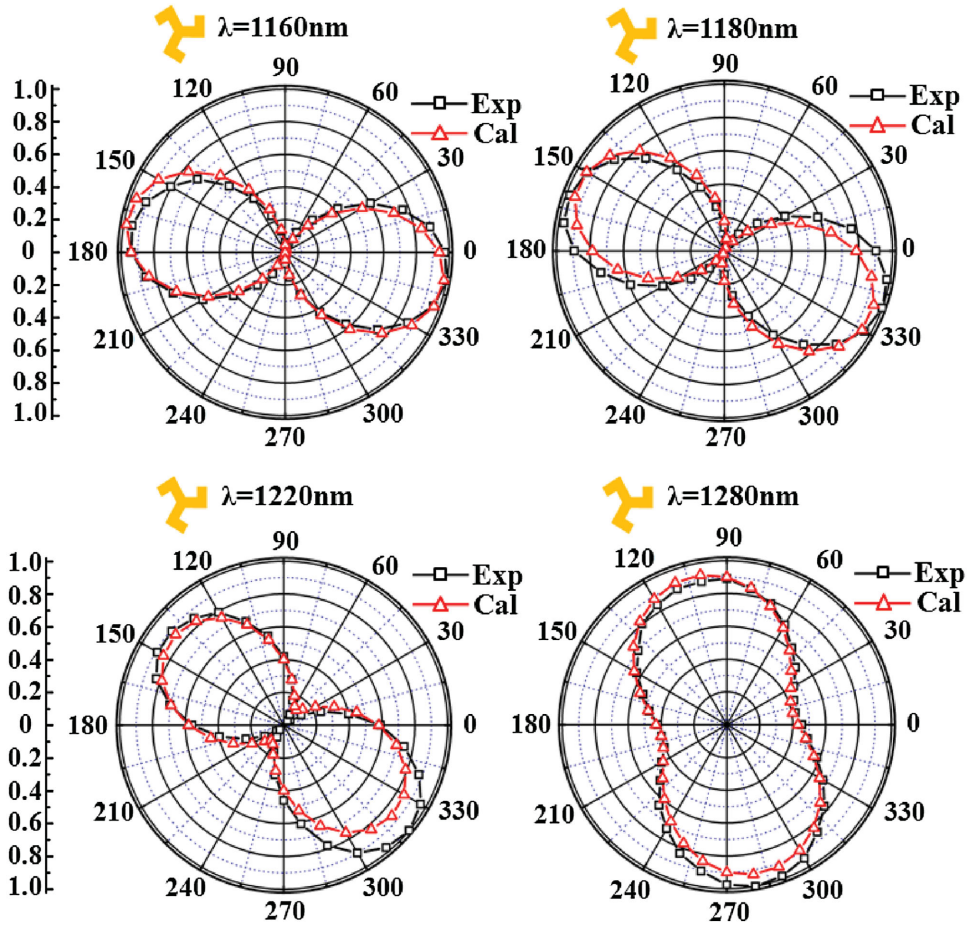

Figure 5. Intensity of the SHG signal as function of the rotation angle of the analyzer for Trisceli-type plasmonic nanostructures. The results are obtained for linearly vertically polarized (V-polarization as shown in Figure 2) illumination at wavelengths of 1160, 1180, 1220, and 1280 nm, respectively. The square and triangular symbols represent the measured (Exp) and calculated (Calc) results. By fitting the measured results, we then experimentally determine the second-order effective susceptibilities of SHG from the Trisceli-type nanostructures.

were focused onto the gold nanostructures from air to glass substrate direction with a spot size of ≈60 μm in diameter. The pulse duration was around 200 fs and averaged power was around 30 mW. After filtering the pumping laser by using short-pass color filters, both the SHG and THG signals were collected by microscope objective lens (20×/NA 0.45) and detected by a grating spectrometer, which was equipped with a cooled Si-CCD as the detector.

Supporting Information

Supporting Information is available from the Wiley Online Library or from the author.

Acknowledgements

S.C., F.Z., and M.W. contributed equally to this work. This work was financially supported by EPSRC (Grant No. EP/J018473/1), Leverhulme (Grant No. RPG-2012-674), and the Deutsche Forschungsgemeinschaft (Grant Nos. TRR142/A05 and ZE953/7-1). M.W. and N.C.P. acknowledge support from European Research Council/ERC Grant Agreement No. ERC-2014-CoG-648328. V.K.V. acknowledges contribution from The Royal Society through a University Research Fellowship. K.W. would like to thank the support from Research Grant Council of Hong Kong under Project AoE/P-02/12. S.Z. acknowledges financial support from the NSFC (Grant No. 61328503).

Received: November 14, 2015
Revised: December 31, 2015
Published online: February 23, 2016

[1] B. M. Maoz, Y. Chaikin, A. B. Tesler, O. Bar Elli, Z. Fan, A. O. Govorov, G. Markovich, *Nano Lett.* **2013**, *13*, 1203.
[2] R. Schreiber, N. Luong, Z. Fan, A. Kuzyk, P. C. Nickels, T. Zhang, D. M. Smith, B. Yurke, W. Kuang, A. O. Govorov, T. Liedl, *Nat. Commun.* **2013**, *4*, 2948.
[3] F. Lu, Y. Tian, M. Liu, D. Su, H. Zhang, A. O. Govorov, O. Gang, *Nano Lett.* **2013**, *13*, 3145.
[4] R. M. Hazen, D. S. Sholl, *Nat. Mater.* **2003**, *2*, 367.
[5] K. H. Ernst, *Phys. Status Solidi B* **2012**, *249*, 2057.
[6] T. Verbiest, M. Kauranen, A. Persoons, *Phys. Rev. Lett.* **1999**, *82*, 3601.
[7] T. Petralli-Mallow, T. M. Wong, J. D. Byers, H. I. Yee, J. M. Hicks, *J. Phys. Chem.* **1993**, *97*, 1383.
[8] J. D. Byers, H. I. Yee, J. M. Hicks, *J. Chem. Phys.* **1994**, *101*, 6233.
[9] J. J. Maki, M. Kauranen, A. Persoons, *Phys. Rev. B* **1995**, *51*, 1425.

[10] T. Verbiest, M. Kauranen, Y. V. Rompaey, A. Persoons, *Phys. Rev. Lett.* **1996**, *77*, 1456.
[11] P. Fischer, in *Comprehensive Chiroptical Spectroscopy, Vol. 1: Instrumentation, Methodologies, and Theoretical Simulations*, (Eds: N. Berova, P. L. Polavarapu, K. Nakanishi, R. W. Woody), John Wiley & Sons, Inc., Hoboken, NJ, USA **2012**.
[12] W. Cai, A. P. Vasudev, M. L. Brongersma, *Science* **2011**, *333*, 1720.
[13] M. Kauranen, A. V. Zayats, *Nat. Photon.* **2012**, *6*, 737.
[14] M. Hentschel, T. Utikal, H. Giessen, M. Lippitz, *Nano Lett.* **2012**, *12*, 3778.
[15] M. Lapine, I. V. Shadrivov, Y. S. Kivshar, *Rev. Mod. Phys.* **2014**, *86*, 1093.
[16] V. K. Valev, A. V. Silhanek, N. Verellen, W. Gillijns, P. Van Dorpe, O. A. Aktsipetrov, G. A. E. Vandenbosch, V. V. Moshchalkov, T. Verbiest, *Phys. Rev. Lett.* **2010**, *104*, 127401.
[17] A. Belardini, M. C. Larciprete, M. Centini, E. Fazio, C. Sibilia, *Phys. Rev. Lett.* **2011**, *107*, 257401.
[18] M. J. Huttunen, G. Bautista, M. Decker, S. Linden, M. Wegener, M. Kauranen, *Opt. Mater. Express* **2011**, *1*, 46.
[19] A. Rose, D. A. Powell, I. V. Shadrivov, D. R. Smith, Y. S. Kivshar, *Phys. Rev. B* **2013**, *88*, 195148.
[20] S. P. Rodrigues, S. Lan, L. Kang, Y. Cui, W. Cai, *Adv. Mater.* **2014**, *26*, 6157.
[21] M. Metzger, L. Gui, J. Fuchs, D. Floess, M. Hentschel, H. Giessen, *Nano. Lett.* **2015**, *15*, 3917.
[22] V. K. Valev, J. J. Baumberg, B. De Clercq, N. Braz, X. Zheng, E. J. Osley, S. Vandendriessche, M. Hojeij, C. Blejean, J. Mertens, C. G. Biris, V. Volskiy, M. Ameloot, Y. Ekinci, G. A. E. Vandenbosch, P. A. Warburton, V. V. Moshchalkov, N. C. Panoiu, T. Verbiest, *Adv. Mater.* **2014**, *26*, 4074.
[23] R. Kolkowski, L. Petti, M. Rippa, C. Lafargue, J. Zyss, *ACS Photon.* **2015**, *2*, 899.
[24] M. Kuwata-Gonokami, N. Saito, Y. Ino, M. Kauranen, K. Jefimovs, T. Vallius, J. Turunen, Y. Svirko, *Phys. Rev. Lett.* **2005**, *95*, 227401.
[25] R. W. Boyd, *Nonlinear Optics*, Academic Press, San Diego, CA, USA **2008**.
[26] S. Bhagavantam, P. Chandrasekhar, *Proc. Indian Acad. Sci. A* **1972**, *76*, 13.
[27] O. E. Alon, V. Averbukh, N. Moiseyev, *Phys. Rev. Lett.* **1998**, *80*, 3743.
[28] K. Konishi, T. Higuchi, J. Li, J. Larsson, S. Ishii, M. Kuwata-Gonokami, *Phys. Rev. Lett.* **2014**, *112*, 135502.
[29] G. X. Li, S. M. Chen, N. Pholchai, W. H. Wong, E. Y. B. Pun, K. W. Cheah, T. Zentgraf, S. Zhang, *Nat. Mater.* **2015**, *14*, 607.
[30] S. M. Chen, G. X. Li, F. Zeuner, W. H. Wong, E. Y. B. Pun, T. Zentgraf, K. W. Cheah, S. Zhang, *Phys. Rev. Lett.* **2014**, *113*, 033901.
[31] S. Sioncke, T. Verbiest, A. Persoons, *Mater. Sci. Eng. R* **2003**, *42*, 115.
[32] M. Weismann, D. F. G. Gallagher, N. C. Panoiu, *J. Opt. Soc. Am. B* **2015**, *32*, 523.
[33] A. A. Shcherbakov, A. V. Tishchenko, *J. Quant. Spectrosc. Radiat. Transfer* **2012**, *113*, 158.
[34] A. V. Andreev, A. A. Korneev, L. S. Mukina, M. M. Nazarov, I. R. Prudnikov, A. P. Shkurinov, *Phys. Rev. B* **2006**, *74*, 235421.
[35] J. I. Jang, S. Mani, J. B. Ketterson, P. Lovera, G. Redmond, *Appl. Phys. Lett.* **2009**, *95*, 221906.
[36] N. Ueda, H. Kawazoe, Y. Watanabe, M. Takata, M. Yamane, K. Kubodera, *Appl. Phys. Lett.* **1991**, *59*, 502.
[37] P. B. Johnson, R. W. Christy, *Phys. Rev. B* **1972**, *6*, 4370.
[38] M. Campoy-Quiles, G. Heliotis, R. Xia, M. Ariu, M. Pintani, P. Etchegoin, D. D. C. Bradley, *Adv. Funct. Mater.* **2005**, *15*, 925.
[39] *Nonlinear Surface Electromagnetic Phenomena* (Eds: T. F. Heinz, H. E. Ponath, G. I. Stegeman), Elsevier, Amsterdam, The Netherlands **1991**, Ch. 5, p. 353.
[40] K. O'Brien, H. Suchowski, J. Rho, A. Salandriona, B. Kante, X. Yin, X. Zhang, *Nat. Mater.* **2015**, *14*, 379.